Laser and Particle Beams (2012), *30*, 341–356.

doi:10.1017/S0263034612000183

Modeling of the plasma produced by moderate energy laser beam interaction with metallic targets: Physics of the phenomena

ISAK I. BEILIS

Electrical Discharge and Plasma Laboratory, School of Electrical Engineering, Fleischman Faculty of Engineering, Tel Aviv University, Tel Aviv, Israel

(Received 2 December 2011; Accepted 14 March 2012)

Abstract

The physical phenomena of plasma plume generation and plasma expansion by target-laser interaction are considered for moderate laser power density. The kinetics of target vaporization, atom ionization, and plasma heating are described. The mechanism of electric sheath formation near the surface, electron emission from the target, and the electrical breakdown phenomena by laser irradiation are analyzed. The plasma expansion is described taking into account the near target plasma structure and the absorption of the laser radiation. The mechanisms accelerating the plasma and generating an electric field in it are discussed. The work reviews experiments and theoretical models and summarizes the results in order to understand the measurements and to discuss open questions. As example, the plasma parameters (electron temperature and density, degree of ionization, and plasma velocity) are calculated for an Ag target using the developed model that considers self-consistently the target heating, kinetics of target evaporation, plasma heating, and ion flux to the target. The calculated ion velocity in the expanding plasma jet is in accordance with the measurement. The ion energy linearly depends on the ion charge state, as observed experimentally.

Keywords: Electron emission; Ion charge; Laser plasma; Plasma expansion; Sheath; Target ablation

1. INTRODUCTION: GENERAL BACKGROUND, MOTIVATION AND APPLICATIONS

Numerous applications indicate that laser-matter interaction is technologically important (Hoffmann *et al.*, 2005). In particular, the interaction of intense laser beams with plasmas is highly relevant to laser fusion (Miller *et al.*, 2004), material science and medicine (Gamaly *et al.*, 2002), and nanoparticles generation (Eliezer *et al.*, 2005). The interferometric diagnostics was established as a technique to probe dense plasmas using optical wavelength laser beams (Attwood *et al.*, 1978). A large electric field can be generated in plasma by high power lasers and used to accelerate electrons (Tajima & Dawson, 1979; Steinke *et al.*, 2010; Shoucri *et al.*, 2011).

One of the important phenomena is plasma generation near a target surface by the impingement of laser radiation of moderate power density (10^6–10^{10} W/cm^2) focused onto a very small area. Such plasmas are used for target surface treatment (Tsue & Redman, 2000; Fernandez *et al.*, 2005), thin film deposition (Anisimov *et al.*, 1993; Gamaly *et al.*, 1999; Singh & Narayan, 1990; Shukla & Khare, 2010), high-energy atomic beam generation (Zheng *et al.*, 1989), laser welding (Moscicki *et al.*, 2006), laser beam machining (Dubey & Yadava, 2008), and ion beam generation (Schaumann *et al.*, 2005).

Several phenomena occur during laser-target interaction (LTI). When the laser pulse is absorbed by the target, energy is converted into thermal and mechanical energy, ablating the target. When the laser pulse is absorbed by the vapor, energy is converted into thermal energy of the vapor particles, and then into plasma formation. Then the laser radiation will interact with the generated plasma. Understanding the physics of energy conversion is useful for choosing the laser and target characteristics suitable for different applications, taking into account ablation. This understanding can be achieved by theoretically modeling laser plasma generation and plasma expansion. The models should be based

Address correspondence and reprint requests to: Isak I. Beilis, Electrical Discharge and Plasma Laboratory, School of Electrical Engineering, Fleischman Faculty of Engineering, Tel Aviv University, P. O. Box 39040, Tel Aviv 69978, Israel. E-mail: beilis@eng.tau.ac.il

on experimental studies of the laser interaction phenomena. Below the state of plasma measurements is discussed to formulate the main problem of moderate power laser interactions with metallic targets and the results are used for laser plasma modeling.

2. REVIEW OF EXPERIMENTAL RESULTS AND MODELS

2.1. Methods and Measurements

A laser pulsed beam with 6-ns pulse durations 3.2 mJ energy impinged on an Al target and modified it. Using scanning electron microscopy Henc-Bartolic *et al.* (2008) observed that molten droplets with radii between 0.1 and 0.5 μm, Al vapor and surface craters of about 30 μm depth were formed after 50 laser pulses. The electron temperature of the Al plasma was estimated as 1.4 eV, using spectroscopic data and that the laser energy was mostly absorbed by the plasma particles. The plasma produced by a pulsed nitrogen laser beam (6 ns, 9 mJ) impinging on a Ti target was studied spectroscopically by Henc-Bartolic *et al.* (1994). It was found that the electron density was $n_e \sim (1.5\text{–}3) \times 10^{18}$ cm^{-3} and that Stark broadening is the dominant broadening mechanism. The electron temperature T_e measured from the relative intensities of two Ti spectral lines in vacuum was approximately 2.7 eV.

Time- and space-resolved spectra were recorded by Hermann *et al.* (1995) to investigate the plasma formed from 20 ns pulsed excimer laser irradiation of Ti targets. The laser intensity was varied from the vaporization threshold at 25 MW/cm^2 up to 500 MW/cm^2, which generated plasma. T_e at distance 2 mm from the target decreased with time, from 2–3 eV at 150 ns after the laser pulse, to 1.5 eV at 300 ns. At fixed time of 100 ns after the laser pulse, density n_e decreased with distance, from 10^{18} cm^3 at 0.5 mm to 10^{17} cm^3 at 2 mm, as measured using the Stark broadening of Ti atom and ion lines. When the power density increased from 25 to 500 MW/cm^2, the directed ion velocity increased from 2×10^5 to 2×10^6 cm/s.

Chang and Warner (1996) used a Cu vapor laser (CVL) and varied the intensity from 0.1 to 10 GW/cm^2 to investigate the parameters of plasma generated from Al and carbon steel targets. Schlieren images were captured by a charge-coupled device. A narrow-band filter centered at the probe laser wavelength was used to block the plume radiation and scattered CVL light. The measured speed $(3\text{–}20) \times 10^5$ cm/s was used to determine vapor density, temperature, and pressure during the end of the CVL pulse through the hydrodynamic relations describing adiabatic shock expansion and Knudsen-layer jump conditions. It was found that T_e was 1–2 eV and $n_e = 10^{20}$–10^{21} cm^{-3}. These data correlated with published measurements even though the reverse approach was uncertain.

The energy distribution of ions ejected from solid and liquid Si and Ge and from solid Cu targets by a high-fluence (1–8) J/cm^2 excimer laser was determined by analyzing the time of flight (TOF), by measuring the current pulse delay of ions overcoming an adjustable electrostatic potential barrier applied before a detector (Franghiadakis *et al.*, 1999). For both solid and liquid targets, the ion energies were found on the order of 100 eV per ion charge and depended little on the laser fluence.

Abdellatif and Imam (2002) determined the spatial distribution of T_e using Boltzmann plots of Al II lines and the spatial profile of n_e using Stark broadening, produced by a 7 ns pulse laser with wavelengths 1064, 532, and 355 nm. When the laser wavelength was 1064 nm, $T_e \sim 1.17$ eV at the target surface, passed maximum (6.3eV), and it increased gradually to 4.2 eV at a distance of 500 mm from the target surface and then decreased with distance to about 1 eV. When the laser wavelength was 355 nm, maximum T_e was about 5.7 eV and $n_e = (0.85\text{–}0.35) \times 10^{18}$ cm^{-3}. Rieger *et al.* (2003) investigated the emission Si and Al plasmas produced by a KrF laser with 10 ps pulse and power densities (0.05–50) GW/cm^2, and also with 50 ps pulse and power densities (10–10^4) GW/cm^2. It was shown that 50 ps, 100 GW/cm^2 pulses generated Al plasma with $n_e \sim 10^{22}$ cm^{-3}, $T_e \sim 14$ eV, while 10 ns, 0.5 GW/cm^2 pulses produced 10^{20} cm^{-3} and ~2.4 eV.

A 7 ns pulsed Nd:YAG laser producing a 52 mJ, 335 nm, 10^{10} W/cm^2 beam was irradiated on a Cu target in vacuum and Ar (Hafez *et al.*, 2003). T_e was determined by a Boltzmann plot and n_e by Stark broadening. Also a single Langmuir probe was located 3.5 mm from the target. In vacuum, T_e increased from 1.6 eV at the surface to 3.8 eV at a distance of 2 mm from the surface, and then decreased, reaching 0.6 eV at 10 mm. The plasma velocity was found as 5.3×10^5 cm/s. The electron density was $n_e \sim 1.4 \times 10^{16}$ cm^{-3} at the surface and decreased by more than one order of magnitude at a distance of 10 mm from the target.

The plasmas produced by a 200 mJ, 8 ns pulse in air on a target from ~60% Cu, ~40% Zn brass alloy was studied spectroscopically (Corsi *et al.*, 2004). It was reported that n_e was 10^{16}–10^{18} cm^3 and T_e 0.7–1.2 eV. Aguilera *et al.* (2004) studied plasma induced by a (3.5–4.5) GW/cm^2, 4.5 ns, laser beam in atmospheric pressure air and Ar and focused onto a Fe target, and determined the temporal and spatial distributions of T_e and n_e and neutral atom density. In air, the Fe emissivity and atom density were maximized when the focal plane of the lens was placed 10 and 12 mm, respectively, below the sample surface, whereas higher temperature (1 eV) was obtained when the focus was 5 mm below the surface and decreased for deeper focusing positions. This behavior is explained by plasma shielding at high laser irradiance. The emission intensity in Ar was about twice of the intensity in air due to higher temperature in Ar. Also, a maximum of the emission intensity was found for both gases at a focus distance of ~10 mm.

Laser generated metallic plasma was widely investigated by Torrisi and co-authors, and the details of their methods were described recently (Margarone *et al.*, 2008; Torrisi

https://doi.org/10.1017/S0263034612000183 Published online by Cambridge University Press

et al., 2008*a*, 2008*b*). They used a Nd:Yag laser with a 3–9 ns pulse and fluence of (0.1–9.3) J/cm^2. Electrostatic ion energy analyzers and the TOF technique were used to measure the ion energy and charge state distributions. The mass loss per pulse was obtained by measuring the crater depth profile. The radiation emission spectrum, T_e and n_e were investigated by optical spectroscopy using a charge-coupled device camera. They found, for metal targets with a wide range of thermophysical properties, that the ion distribution function was a shifted Maxwellian distribution, which depended on laser fluence, and that the energy shift increased linearly with the ion charge. For carbon it was about 65 eV/charge (Torrisi *et al.*, 2006) and for Si about 300 eV/charge, with ion charge from +1 to +4 at 150 mJ laser energy (Torrisi *et al.*, 2008*a*, 2008*b*). Using the maximal energy ion distribution shift the estimated singly charged ion velocity for carbon was 2.8×10^6 cm/s and for Si was 4.5×10^6 cm/s. The energy shift increase with the ion charge was explained assuming that an electrostatic field is present within a Debye length similarly with that electric field occurred for high intensity fs and ps laser pulse irradiation.

For Ta, the ion energy was higher, about 200 eV/charge at 30 J/cm^2 and about 600 eV/charge state at 100 J/cm^2 (Torrisi *et al.*, 2002). The average width of the distribution indicated a relatively large ion temperature, $(7–26)\times10^5$K, i.e., about 60–200 eV, while the average plasma velocity was reported as $(0.7–1.4)\times10^6$ cm/s. Later for Ag plasma spectroscopic was obtained $T_e\sim5$ eV and $n_e\sim2\times10^{16}$ cm^{-3} (Margarone *et al.*, 2008). Similarly shifted Maxwellian ion distributions were observed by Bleiner *et al.* (2007). The average width of the distribution indicated ion temperature depended on the target material: 18, 27, 30, and 45 eV for Al, Fe, Sn, and Zn, respectively.

Torrisi *et al.* (2000, 2001) measured the target mass loss from the craters by weighing the targets before and after irradiation by 1000 pulses of 9 ns, 875 mJ, and found 0.25, 0.51, 0.55, and 10.5 μg/pulse for Cu, Al, Ni, and Pb, respectively. Another group of materials, Au, Ti, W, and Ta, had higher mass loss (except for Pb), 0.8–1 μg/pulse. A linear dependence of mass loss on fluency in range of 1–6 J/cm^2 was measured for Al, Cu, and Ta targets (Caridi *et al.*, 2006). Kasperczuk *et al.* (2008) showed that the craters have a semi-toroidal shape when the laser was focused inside of the target, and when the laser was focused at the front position they resemble a hemisphere.

Zeng *et al.* (2006) spectroscopically measured T_e and n_e in plasma produced by ns laser impinging on Si target with a flat surface or cavity. T_e was 3eV, about 4eV and n_e was about 5×10^{18} cm^{-3}, $(1–3)\times10^{19}$ cm^{-3} with flat surface and cavity, respectively. T_e and n_e spatial distributions were uniform up to 1.5 mm from the target surface. The plasma expanded at a velocity of 5×10^5 cm/s.

The spatial evolution of T_e and n_e in plasma generated on SiC samples by a Nd:YAG laser beam at wave length of 1064 nm, pulse width of 10 ns, and power of 0.2–2 GW, was spectroscopically studied by Chen *et al.* (2008). They found that n_e decreased from 1.8 to 0.73×10^{17} cm^{-3} and T_e from 1.4–1.7 to 1 eV with distance from the target up to 9 mm. In the region between 3–9 mm, n_e fluctuated and T_e decreased slowly. Further investigations of these authors determined the T_e and n_e dependence on the time after the pulse (Chen *et al.*, 2009*a*, 2009*b*; Sun *et al.*, 2008). It was shown that T_e substantially and n_e moderately decreased with time in range of 50–600 ns. For example, at 1 mm from the target surface, T_e decreased from 3.3 to 1.75 eV and n_e decreased from 2.6×10^{17} to 2.25×10^{17} cm^{-3} at 50 and 400 ns respectively after the laser pulse. T_e and n_e had maxima at about 2 mm from the target surface.

Cristoforetti *et al.* (2009) spectroscopically observed that n_e increased from 0.7×10^{16} to 2×10^{17} cm^{-3} and T_e from 0.85 to 1.15 eV when the irradiance of a Nd:YAG laser beam of Al target increased from 3×10^8 to 5×10^9 Wcm^2. Ablated plasma flow from a liquid Ga-In target was studied with laser power density 1 GW/cm^2 and pulse duration 2.7 ns (Popov *et al.*, 2011). The average ion energy and the directed ion velocity were measured using a mass-energy and TOF methods, respectively. The found energy of about 400 eV, indicating that there was an electrostatic field in the plasma plume. However, a relatively low velocity of about 3×10^5 cm/s was measured. Measured characteristic plasma parameters published in last decades are summarized in Table 1.

2.2. Laser Plasma Plume Models

Material ablated from the target from the impingement of a laser beam expands away from the surface in form of a plasma jet. Jet expansion into vacuum is described by the hydrodynamaic equations, expressing the conservation of mass, momentum, and energy. Gamaly *et al.* (2005) showed that with ps pulses the ablation threshold of laser irradiation in air is significantly lower than in vacuum. Plasma formation by the impingement of nanosecond (3–7) J/cm^2 pulsed laser beams on Cu, Ba, and Y targets was modeled by Singh and Narayan (1990). The assumed equilibrium, with T_e equal to the heavy particle temperature T, isothermal expansion during the pulse action and adiabatic plasma expansion after the pulse. The dynamics of thin film laser deposition was obtained using the time evolution of the calculated plasma velocity and measured T_e.

Bogaerts *et al.* (2003) and Chen *et al.* (2005) proposed a one-dimensional transient system of equation for equilibrium plasma and Moscicki *et al.* (2006) proposed a two-dimensional approach. Non-equilibrium (i.e., $T_e \neq T$) plasma expansion was simulated by Itina *et al.* (2002). A three-dimensional computer code was used by Wang and Chen (2003) to solve the hydrodynamic governing equations, to study the plasma plume characteristics in laser welding for iron vapor in an ambient gas. The temperature, vapor, and gas velocity as boundary conditions at the target were used as parameters. An important part of LTI study is to correctly define the temperature dependent boundary conditions at the

https://doi.org/10.1017/S0263034612000183 Published online by Cambridge University Press

Table 1. *The methods and measured characteristic plasma parameters (ion velocity and energy, electron temperature and density) depending on laser type, power, pulse duration and spot area in experiments with laser irradiation of the different target materials.*

Target	Laser	Pulse, ns	Energy, Fluence	Spot diameter, Area	Method	V, cm/s	Ne, cm^{-3} Craters	Te eV	Shift, V/charge	Reference
Ti	excimer laser	20	25–500 MW/cm^2		TOF, Stark broadening	$(0.2–1)\times10^6$	10^{18}–10^{17}	3–1.5	—	Hermann *et al.* (1995)
Si, Ge, Cu	excimer-laser	25	(1-8) J/cm^2		Electrostatic analyzer TOF	$(1.8–3.1)\times10^6$	10^9 Ions/pulse	2	100	Franghiadakis *et al.* (1999)
Al & carbon steel	Cu-laser		0.1 to 10 GW/cm^2		CCD camera	$(3–20)\times10^5$	10^{20}–10^{21}	1–2	—	Chang and Warner (1996)
Ti	N_2-laser	6	9 mJ	—	Stark broadening	—	$(1.5–3)\times10^{18}$	2.7	—	Henc-Bartolic *et al.* (1994)
Al	N_2-laser	6	3.2 mJ	—	SEM	—	Droplets 0.1–0.5 μm Craters 30 μm	1.4 (estimated)	—	Henc-Bartolic *et al.* (2008)
Ta	Nd:YAG wavelengths 1064	9	1–900 mJ	0.5 mm^2	Electrostatic analyzer TOF	1.6×10^6	—	—	200–600	Torrisi *et al.* (2002)
Al	Nd:YAG wavelengths 1064, 532 & 355 nm	7	500, 100, and 60 mJ	300 μm	Boltzmann plot, Stark broadening	—	$(0.85–0.35)\times10^{18}$	1.17–6.3	—	Abdellatif and Imam (2002)
Al, Si	KrF laser	50 ps–10 ns	(0.05–50) & 10000 GW/cm^2	5 μm	Spectra Pro 500	—	10^{20}– 10^{22}	2.4–14	—	Rieger *et al.* (2003)
Cu	Nd :YAG wavelengths 335 nm,	7	52 mJ	10^{10} W/cm^{-2}	Spectroscopy CCD camera, Langmuir single probe	5.3×10^5	1.4×10^{16}	1.6–0.6 at 10 mm $T_{e\ max}$ = 3.8 eV at 2 mm	—	Hafez *et al.* (2003)
Fe	Nd:YAG 1064 nm	4.5	100 mJ	(3.5–4.5) GW/cm^2	Spectrometer CCD	—	2×10^{16}	1.0	—	Aguilera *et al.* (2004)
60%Cu,~40% Zn brass	Nd:YAG 1.06 μm	8	200 mJ	—	Echelle type spectrometer CCD camera	—	10^{16} –10^{18}	0.7–1.2	—	Corsi *et al.* (2004)
Pyrolytic graphite	Nd:Yag 532 nm	3	20–170 mJ	Area 3 mm^2	Quadrupole spectrometer	2.8×10^6 estimated	6.7×10^{17}	—	65	Torrisi *et al.* (2006)
Al, Cu and Ta	Nd:Yag 532 nm	3	1.7–170 mJ	Area 0.8 mm^2	Quadrupole spectrometer	_	—	—	83 & 112	Caridi *et al.* (2006)
Si	Nd:Yag 266 nm	3	40 J/cm^2	40 μm	spectroscopic measurements	2×10^6	$(0.5–3)\times10^{19}$	~5	—	Zeng *et al.* (2006)
Al, Fe, Sn, Zn	Eximer 248 mm	23	1.3 GW/cm^2	Area 1 mm^2	Faraday cup TOF	$(2–4)\times10^6$	—	Width:18,27,30,45 eV	—	Bleiner *et al.* (2007)
Si	Nd:Yag 532 nm	3	25–150 mJ	Area 0.5mm^2	Quadrupole spectrometer TOF	4×10^6 estimated	—	6–9 (estimated)	259–306	Torrisi *et al.* (2008*a*, 2008*b*)

Ag	Nd:Yag 1064 nm	3-9	(0.3 – 9.3) J/cm^2	Area 3 mm^2	Spectroscopy TOF energy analyzer,	10^6	2×10^{16}	5	280	Margarone *et al.* (2008)
Al,Zn,Pb,Ta	Nd:Yag 532 nm	3	50–150 mJ	Area 2 mm^2	Electrostatic mass spectrometer	—	—	—	80, 90, 95 115 — Pb, Zn, Al Ta	Torrisi *et al.* (2008*a*, 2008*b*)
SiC	Nd:YAG 1064 nm	10	1.9–11 mJ	1 mm	Spectroscopic Boltzmann plot, CCD	—	$(1.8–0.73)\times10^{17}$	1.1–1.6	—	Chen *et al.* (2008)
SiC Time delay 50-400ns	Nd:YAG 1064 nm	10	130	1 mm	Spectroscopic Boltzmann plot, CCD	—	$(3–1)\times10^{17}$	3.5–1	—	Chen *et al.* (2009)
$KTiOAsO_4$ At distance 1-19mm Time delay 50-600ns	Nd:YAG 1064 nm 532 nm	10	1.9–11 mJ	1 mm	Spectroscopic Boltzmann plot, Stark CCD	—	$(2.9–1.55)\times10^{17}$ $(3.5–0.7)\times10^{17}$	3–0.7 2.2–1.5	—	Sun *et al.* (2008) Chen *et al.* (2009)
Al	Nd :YAG 1.06 μm	32	2.6–38 mJ	$(0.3–5)\times10^9$ Wcm^2	Echelle type spectrometer CCD camera	—	$(0.07–2)\times10^{17}$	0.85–1.15	—	Cristoforetti *et al.* (2009)
Ga-In	Nd:YAG 1064 nm	2.7	1 GW/cm^2	100 μm	mass-energy analyzer, TOF	3×10^6	—	—	Effective energy, 400 eV	Popov *et al.* (2011)

target-plasma interface. A model of laser ablation in an ambient gas taking into account the phenomena of target-vapor interaction was proposed by Gusarov *et al.* (2000) and Gusarov and Aoki (2005). A weakly ionized vapor was considered, and the given plasma pressure at the target-plasma kinetic boundary was used as a parameter, assuming plasma equilibrium (i.e., $T_e = T$).

Cathode spot theory (Beilis, 2001) was modified for current-less laser generated plasma flow (Beilis, 2006). This model takes in account non-equilibrium plasma flow and a jump of plasma parameters in the Knudsen layer, at the solid surface-plasma interface self-consistently. The mechanism of near-target laser plasma generation and flow using the kinetics of target vaporization, plasma heating and atom ionization was considered self-consistently in a mathematical model without arbitrary given parameters (Beilis, 2007).

2.3. Review Summary

When the laser power density exceeds 10^8 W/cm^2, the plasma was produced with broad ion kinetic energy distributions. Furthermore, when multiply charged ions are detected, it was found that their most probable kinetic energy increases linearly with the ion charge. This energy reaches few hundred eV per ion charge, and was identified with a correspondingly large potential drop in the plasma, which was not always correlated with the moderate plasma velocities $(5–20)\times10^5$ cm/s that were observed by TOF. Also, the electron temperature was usually low, 1–2 eV, and the direct spectroscopic measurements never exceeded 5–6 eV, while the measured average width of the ion velocity distribution function corresponded to relatively large plasma temperatures, reaching few tens eV depending on target material and laser fluence.

While these measured plasma parameters were briefly explained in the discussions in the experimental papers, they only considered separate phenomena and were usually based on comparison with other observations. The mechanism of ion acceleration for high power ($>10^{14}$ W/cm^2) laser impingement was used to explain the ion energy measured by the moderate laser power irradiation. Why the relatively large measured ion energies were not correlated with the low spectroscopically measured electron temperatures was not explained. In the theoretical works, the calculated results for moderate power density were obtained using some arbitrary parameters. Mostly the calculated results agreed with the measured low electron temperatures and plasma velocities. However, multicharged (>2) ion generation and the ion energy dependence on charge in the expanding plasma was not considered. Thus, understanding of the measured results requests to consider the LTI as mutually dependent phenomena.

2.4. Objective and Organization

The objective of this paper is to clarify the tractability of moderate energy LTI measurements considering the coupled

https://doi.org/10.1017/S0263034612000183 Published online by Cambridge University Press

physical phenomena determined the produced laser plasma parameters as ion energy, plasma temperature, etc. To this end, the physics of laser ablation and plasma generation will be considered, taking into account the kinetics near the target-plasma interface, the hydrodynamics of plasma flow based on existing mechanisms of plasma acceleration, and using a previously developed self-consistent approach to LTI. Therefore the phenomena description will be detailed separately (Section 3) to base the developed plasma model for LTI. Thus, LTI is studied by analyzing target vaporization (Section 3.1), considering vapor breakdown mechanisms (Section 3.2), sheath formation (Section 3.3), electron emission (Section 3.4), and mechanism of plasma heating (Section 3.5). Section 4 models the plasma expansion and Section 5 describes the existing mechanisms of plasma acceleration. The application of laser plasma model and calculating results will be presented in Section 6. The calculated results and the possible nature of ion energy distribution and the energy dependence on ion charge by LTI will be discussed and summarized in Section 7.

3. NEAR-TARGET PHENOMENA

The pulsed laser ablation and plasma formation is complex and various phenomena occur. Below these phenomena are analyzed separately using the known data to their involving self-consistently by the laser plasma modeling.

3.1. Target Ablation

Let us consider the target evaporation and furthermore heavy particle flow. Assuming that the rates of atom condensation and evaporation were equal, Langmuir and Mackay (1914) obtained that evaporated atomic flux density W_L into vacuum is determined by the equilibrium vapor pressure P as $W_L = P/(2\pi mkT_0)^{0.5}$, where m is the atom mass, k is the Boltzmann's constant, and T_0 K is the surface temperature. However, for relatively large T_0, collisions produce a non-equilibrium layer of several mean free path lengths where the atoms are returned back to the surface, and therefore the net rate of material evaporation is less than that into vacuum. Knudsen (1915) showed that a kinetic treatment is required due to non-equilibrium effects. The particle distribution function approaches equilibrium at the external boundary of the *Knudsen layer* or *atom relaxation zone*. Collisions in the vapor force the distribution function (DF) toward a Maxwellian form. Thus two regions appear near the surface: (1) a non-equilibrium region with rare collisions near the target surface and (2) a collision dominated region with hydrodynamic vapor flow. A kinetic approach was used to solve the Boltzmann equation and thus to determine the flow density n, temperature T, and flow velocity u in the non-equilibrium region. These parameters at the external boundary of the Knudsen layer determine the boundary condition for the hydrodynamic flow along a path from the surface. Bhatnagar *et al.* (1954) modeled the collision term in the Boltzmann equation assuming a constant collision time τ, called the relaxation model, in form

$$\frac{\partial f}{\partial t} + \mathbf{v}\frac{\partial f}{\partial \mathrm{r}} = \frac{f_0 - f}{\tau}, \tag{1}$$

where $\boldsymbol{v}$ is the velocity vector, $\boldsymbol{r}$ is the spatial coordinate, f is the DF, f_0 is the local equilibrium distribution function. A steady state one-dimensional problem was considered when the characteristic time of the hydrodynamic parameter set is smaller than the characteristic time of change the heat flux to the surface (Anisimov *et al.*, 1971):

$$v\frac{\partial f}{\partial x} = \frac{f_0 - f}{\tau}, \tag{2}$$

Boundary conditions:

$$f_0 = n_0\left(\frac{m}{\pi 2kT_0}\right)^{3/2}\exp\left[-\frac{mv^2}{2kT_0}\right] \quad v > 0 \quad \text{at} \quad x = 0 \tag{3}$$

$$f_\infty = n_\infty\left(\frac{m}{\pi 2kT_\infty}\right)^{3/2}\exp\left[-\frac{m}{2kT_\infty}((v_x - u)^2 + v_y^2 + v_z^2)\right].$$

at the equilibrium side (∞). The evaporated atoms have a half-Maxwellian DF (f_0) with the surface temperature and density, which is the boundary condition at the evaporated surface $x = 0$. Eqs. (2) and (3) were solved by different approaches. Anisimov (1968) considers the non-equilibrium layer as a discontinuity surface in the treatment of expanded vapor in LTI similar to the shock wave problem. Assuming sonic velocity $u = u_{sn}$, i.e., Mach number M = 1, at the external boundary of the Knudsen layer he obtained an evaporated atom flux of about 0.82 W_L. Fisher (1976) solved the kinetic problem using the BGK approach and obtained that the rate of evaporation into an infinite half-space is about 0.85 W_L.

Laser-induced vaporization of Al and iron targets in air at atmospheric pressure was studied by Aden *et al.* (1990). It was shown that $u = u_{sn}$ is an upper bound for the vapor velocity and for an absorbed intensity the vaporization is independent of the ambient gas. However, in general, the vaporization depends on the ambient pressure, which determines the flow properties in the Knudsen layer. Electrode vaporization into electrical arc plasma, taking into account also electron emission, was treated kinetically by Beilis (1982, 1985, 1986). The definition of plasma flow as a *non-free* (*impeded*) when $M < 1$ and as *free* into vacuum when $M = 1$ was introduced by Beilis (1985, 1986). A strongly impeded mass flow was obtained in cathode evaporation in a vacuum arc due to energy dissipation in the dense plasma. The condition for impeded plasma flow was studied in the case of Teflon propellant in thrusters by Keidar *et al.* (2001). Thus, the vaporized material and the structure of the Knudsen layer are determined the vapor flow and can be taken into account to describe with Eqs. (1)–(3) the laser plasma formation after the electrical breakdown in the vapor.

https://doi.org/10.1017/S0263034612000183 Published online by Cambridge University Press

3.2. Breakdown of Neutral Vapor

Gas breakdown by laser irradiation was discovered in 1962–1963 and found to be similar to spark discharges (Raizer, 1965). The electrical breakdown occurs when an electric field of 3×10^6–10^7 V/cm, depending on the pressure and gas, was produced by the light wave, which can be reached in laser radiation with power density of 10^{10}–10^{11} W/cm^2 (Raizer, 1980). The atoms can be directly ionized by the quantum or the multi-quantum photo-effect and by excited atom ionization by energetic electrons. Also atoms can be ionized by a mechanism, similar to the tunneling effect, i.e., an electron emitted from the atom by a static electric field. The breakdown develops by electron avalanches created by the primary electrons. The gas breaks down when the laser power density exceeds some threshold value. The threshold breakdown electric field for a 50 ns, 30 MW laser beam as a function of Ar, He, and N pressure was measured by Gili and Dougal (1965). Minimum breakdown fields have been found taking into account the electron impact ionization and electron heating through energy transfer from laser light wave to the electrons.

The breakdown threshold laser intensity is lower for plasma generation in metallic vapor due to the lower ionization and excitation energies of metal atoms, compared to gas atoms. This threshold intensity determined by a mathematical model as a function of the laser wavelength (Mazhukin *et al.*, 2003). Mathematical modeling with the given shape and duration of the pulse showed that the threshold intensity of the radiation was 2×10^7 W/cm^2, and the optical breakdown time did not exceed 30 ns. This time reduced to about 10 ns for about 10^9 W/cm^2. The phenomenon was studied considering charged particle generation kinetics, and taking into account different atom ionization mechanisms. However target heating and evaporation was not considered explicitly.

Rosen *et al.* (1982) studied the optical breakdown in Al vapor by excimer laser radiation where the laser threshold intensity for a 0.5 μs pulse was 5×10^7 W/cm^2. The vapor breaks down at shorter times with laser power density. The experimental result was found in good agreement with predicted by a model for plasma initiation included evaporation, photoionization, atom excitation, and others. Thus, the plasma was initiated during time comparable with the regular small laser pulse time for laser power significantly larger then the threshold laser intensity.

3.3. Near Target Electrical Sheath

There is a collisionless sheath between the quasi-neutral plasma and the electrode (Langmuir, 1929). The ions flowing into the sheath from the plasma have a velocity V_i at the sheath boundary, which Bohm (1949) showed must fulfill the condition that $V_i \geq (T_e/m_i)^{0.5}$ in order for the sheath to be stable. The importance of this problem motivated much useful research where different plasma conditions, including the relation between mean free path of different charged particles and the Debye length, were analyzed in order to understand the density, potential and electric field distribution. Franklin (2003) published a general comprehensive review and Eliezer and Hora (1988) reviewed the problem for laser produced plasma.

The plasma-wall transition was studied for electrical discharges by Beilis *et al.* (1998) and Keidar and Beilis (2005). It was shown that the Boltzmann electron distribution cannot be used and that V_i can be lower than Bohm velocity when an oblique magnetic field was applied. In laser generated plasma, the target-plasma transition comprises a sheath formed by plasma floating potential with respect to a negatively charged wall. The sheath should be taken in account considering the LTI (Gusarov & Aoki, 2005). The self consistent study of LTI showed that the ion and electron fluxes across the sheath with potential drop U_{sh} determined the back energy flux to the target previously absorbed in the plasma by laser irradiation (Beilis, 2006) (see below).

3.4. Electron Emission

During LTI, targets are irradiated by highly energetic photons that transport substantial heat flux and an electric field is generated in the sheath at the target-plasma interface. Electrons are emitted from the target by several mechanisms including photo-emission, thermionic (T) emission, field emission by electron tunneling (F), and combined thermal and field (T-F) emission. The photo-effect and electron emission current was generated by ultraviolet laser action on Zn target (Caretto *et al.*, 2007). Relatively low laser power density about 1 MW/cm^2 was studied when mainly photoelectric mechanism determined the electron emission. Dolan and Dyke (1954) calculated the energy distribution of emitted electrons for different temperatures T and electric fields E. Beilis (1974, p. 257) developed this method showing the transition from T- to F-emission and the intermediate case. According to the calculations, electron emission by T- and T-F emission mechanisms can be important for laser power density $>10^7$ W/cm^2.

3.5. Plasma Heating: Electron Temperature

An important question is how the plasma can be heated and what is the mechanism of energy transfer to the electrons by laser irradiation? According to Raizer (1965) plasma electrons can acquire energy in a laser radiation field. Energy absorption from the field is quantum-like. Electrons can acquire instantaneously a large amount of energy from the field from collisions of many photons (Raizer, 1980). Energy absorption is frequency-dependent. Photon energy is absorbed by free electrons the inverse Bremsstrahlung process, producing higher energy free electrons. Previously was shown another mechanism which is due to acceleration of the electron emission in the near target sheath. The energy acquired by the electron beam heated the plasma electrons in an electron beam relaxation region (Beilis, 2006). The electron energy,

https://doi.org/10.1017/S0263034612000183 Published online by Cambridge University Press

absorbed from the field electron beam, is lost via atom excitation, ionization and plasma outflow. Thus, the electron temperature T_e is determined by a balance between energy gain and energy loss which will be used by LTI mathematical description.

4. PLASMA PLUME MODEL

Laser plasma expansion is mathematically described based on a laser-target interaction model (Beilis, 2007) and a modified cathode jet model (Beilis, 2003). The different physical regions in which the described above phenomena occur is schematically presented in Figure 1. The LTI specifically takes into account that the target is heated by laser irradiation and also by incident ions with current density j_i, which transports energy flux $j_i U_{sh}$ acquired in an electrical sheath, and by an electron flow from the plasma with current density j_{et}. The target is cooled by electron emission and thermal conduction into the body of the target. The thermal conduction was determined by solving the transient three-dimensional heat conduction equation (Beilis, 1995, 2007).

The electron emission with current density j_{em} and mass flux G (g/s) emitted from the target is taken in account assuming plasma expansion in the geometrical form of a truncated cone (Fig. 1) with cross-section F depending on distance from the target x (Beilis, 2003). The plasma parameters can be described by a set of hydrodynamic equations of mass, momentum and energy conservation in the expanding plasma flow in 2D approximation developed by Keidar and Beilis (1996). This approach assumes a nearly uniform radial plasma distribution in the expanding jet (Keidar *et al.*, 1996) and therefore the following quasi-one-dimensional system of first-order equations may be presented as:

(1) *Continuity, Momentum and Energy of Ionized Vapor Flow*:

$$\frac{d}{dx}(mn_h VF) = 0, \quad mn_h VF = G \quad n_h = n_a + n_i, \tag{4}$$

$$\frac{d}{dx}(PF + GV) = FeE_p(n_i - n_e), \quad P = n_h kT + n_e T_e, \quad T_i = T_a = T, \tag{5}$$

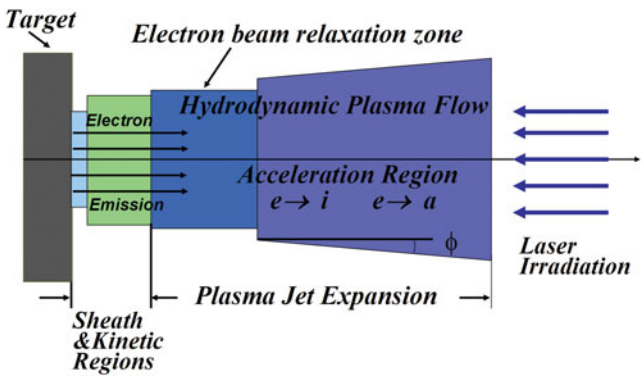

Fig. 1. (Color online) Schematic presentation of the characteristic regions of laser plasma expansion.

$$2n_h Vk\frac{dT}{dx} = kTV\frac{dn_h}{dx} + en_i VE_p + \frac{3\varepsilon n_e k(T_e - T)}{\tau_{ef}} \qquad \varepsilon = m_e/m. \tag{6}$$

(2) *Electron Energy*:

$$\frac{3}{2}n_e V\frac{dT_e}{dx} = \frac{U_{sh}}{F}\frac{d(j_{em}F)}{dx} - \frac{n_e T_e}{F}\frac{d(VF)}{dx} - \frac{U_i}{F}\frac{d(n_i VF)}{dx} - \frac{3\varepsilon n_e(T_e - kT)}{\tau_{ef}} + \alpha_{IB}(x)q_L(x), \tag{7}$$

$$j_{em} + j_i - j_{et} = 0; \qquad q_L(x) = q_L \exp(-(\alpha_{IB}(x)(L_{ef} - x)),$$

$$U_{sh} = T_e Ln\left(0.6\sqrt{\frac{2\pi m_e}{m}} + \frac{j_{em}}{en_{es}}\sqrt{\frac{2\pi m_e}{T_e}}\right)^{-1}.$$

The main mechanism of energy absorption in the plasma and therefore electron heating is inverse Bremsstrahlung. The inverse bremsstrahlung coefficient $\alpha_{IB}(x)$ is determined by the laser wave length λ, and depends on distance x from the target and can be calculated as (Singh & Narayan, 1990):

$$\alpha_{IB}(x) = 3.69 \times 10^8 \frac{Z^3 n(x)^2 \lambda^3}{c^3\sqrt{T_e(x)^o K}}\left(1 - \exp\left(-\frac{hc}{\lambda k T_e(x)^0 K}\right)\right).$$

(3) *Ion Continuity*:

$$\frac{1}{F}\frac{d(n_i VF)}{dx} = S_e; \quad S_e = \beta_i n_e n_a - \beta_r n_i n_e^2. \tag{8}$$

(4) *Electron continuity*:

$$\frac{1}{eF}\frac{d((j_{em}(x) + en_e V)F)}{dx} = -S_e, \qquad j_{em}(x) = j_{em}(0)\exp(-(\sigma_i n_a + \sigma_c n_e)x). \tag{9}$$

(5) *Electric Field*:

$$\frac{\varepsilon_0}{F}\frac{d(FE_p)}{dx} = e(n_i - n_e), \tag{10}$$

where q_L is the laser power density, n_h is the heavy particle density, τ_{ef} is the effective time between electron-ion and electron-atom collisions, n_e and n_i are ion and electron densities, respectively, n_{es} is the equilibrium plasma density at the sheath edge, β_i and β_r are the coefficients of ionization and recombination, h is the Plank constant, T_e is the electron temperature in eV, T(°K) is the heavy particle temperature, σ_i and σ_c are the cross-sections of atom ionization and Coulomb collisions, respectively, ε_o is the vacuum permittivity, U_i is the atomic ionization energy, E_p is the electric field in the plasma, and L_{ef} is an effective dense plasma length.

Eqs. (8) and (9) take in account that the atoms are ionized by the emitted electron beam with current density j_{em} and by the plasma electrons with T_e. Usually the plasma is quasineutral ($n_e \approx n_i = n$), and E_p is determined by the gradient of the

https://doi.org/10.1017/S0263034612000183 Published online by Cambridge University Press

electron pressure (see below Eq. (12)). A deviation from quasi-neutrality is possible in the flow far from the surface at the front of the expanding plasma where a large electric field E_p can be induced (see Section 5). In this case, E_p can be estimated from Eq. (5) and Eq. (10). The above system of equations can be solved using the boundary conditions described in Section 3.1 and developed for laser generated plasma near the target surface (Beilis, 2007).

5. PLASMA ACCELERATION MECHANISM

Let us consider the possible mechanisms for accelerating fully ionized plasma having conductivity σ. The equation of ion motion in general form is:

$$m\frac{d\vec{V}_i}{dt} = -\frac{\nabla P_i}{n_i} - \frac{e\vec{j}}{\sigma} + e(E + [\vec{V}\vec{H}]/c), \tag{11}$$

where P_i is the ion pressure, V_i is the ion velocity, j is the electrical current density, and $\vec{H}$ is the magnetic field vector. The electric field E is limited by high electron mobility in a quasi-neutral plasma. In order to study the electrical field generation mechanisms while maintaining quasi-neutrality, the equation of electron motion with velocity V_e and pressure P_e may be considered in the following form:

$$e\left(E - \frac{\vec{j}}{\sigma}\right) = -\frac{\nabla P_e}{n_e} - \frac{md\vec{V}_e}{dt} - \frac{e}{c}[\vec{V}_e\vec{H}]. \tag{12}$$

The sum of Eqs. (11) and (12) in simple case where $H = 0$ and $j = 0$ for moderate laser power is:

$$m\frac{dV_i}{dt} = -\frac{\nabla(P_i + P_e)}{n_i} - m\frac{d\vec{V}_e}{dt}. \tag{13}$$

Considering Eq. (13), the following forces accelerating the plasma can be noted: (1) Forces due to gradient of charged particle density and by particle heating in the flow when the inertial term of electrons can be neglected. This is the *gas dynamic* or heat mechanism (see Section 4). (2) Electron inertia—from the last term in eq (13):

$$E \approx \frac{m_e}{e}\frac{d\vec{V}_e}{dt}. \tag{14}$$

This mechanism contributes with strong V_e variation in a small time. For example, when an electron velocity increases to 5×10^7 cm/s in 0.1 ns the electrical field of about 280 V/cm can be induced. (3) Force in the rarefied part of the expanding plasma caused by an *electric field at the plasma front* due to significantly fast motion of the hot electrons in comparison with the ions, and resulting in a strong violation of quasi-neutrality (see also Eq. (5)). The ions stream into vacuum with electrons, preceded by a characteristic length at which a space charge can be induced. This space charge at the boundary of the expanding plasma produces the accelerating electrostatic field at the ion front. The most energetic electrons extend into vacuum, maintaining an accelerating field determined by the electron temperature.

Eliezer and Ludmirsky (1983) estimated electric fields between about 5×10^5 to 5×10^6 V/cm at widths from 10 to 100 Debye lengths for a sheath produced by Nd:YAG laser intensities between 10^{12} to 10^{15} W/cm^2. The ion acceleration with the electrostatic field E caused by the hot electrons in the freely expanding plasma model was considered by Denavit (1979). This approach was extended by Wilks *et al.* (2001) in frame of target normal sheath acceleration (TNSA) model. The expanding ions were described by the ion continuity and motion equations taking into account the electron-ion interaction. The electrons were assumed to be in isothermal equilibrium and given by the Boltzmann relation taking into account the quasi-neutrality of the plasma plume. A self-similar solution gives $E = T_e/L$; $L = V_s t$, where V_s is the ion sound speed and t is the characteristic acceleration time. Pearlman and Morse (1978) take in account effect of the truncation of the electron Maxwellian distribution and they showed that the maximal ion velocity reached when the Debye length equals the density scale length L. Thus, in essence acceleration of the ions due to the electron temperature gradient was considered. The problem of ion acceleration in a time-dependent ambipolar field was developed for the case when the electron energy strongly depends on time during a powerful subpicosecond laser pulse (Gamaly, 1993). A significant difference with the well-known case of isothermal expansion was observed (Wickens *et al.*, 1978).

The shifted Maxwellian ion energy distribution measured for relatively moderate laser power density ($\leq 10^{10}$ W/cm^2) was proposed to explain by ion acceleration in an electric field estimated as the measured equivalent voltage ratio to the Debye length (Torrisi & Gammino, 2006). It was indicated that this electric field is in accordance with that obtained in $(1–5) \times 10^{19}$ W/cm^2, fs and ps pulse experiments (Devies *et al.*, 1999; Pukhov, 2001; Hegelich *et al.*, 2002). The electrostatic field model for ion acceleration was developed by Hatchett *et al.* (2000) with scale length L given by the Debye length. Using one- and two-dimensional numerical simulations, Wilks *et al.* (2001) indicated that the electrostatic acceleration mechanism (also called TNSA), is applicable only for ultra-intense (10^{17}–10^{20} W/cm^2), short-pulse (fs and ps) lasers when $T_e \sim$MeV and $L \sim 10$ μm.

Liseikina *et al.* (2008) indicated that in contrast to the TNSA mechanism used to explain most of the experiments with ion acceleration from solid targets, laser radiation pressure acceleration (RPA), predicted from theoretical studies, becomes dominant at intensities exceeding 10^{23} W/cm^2 and produces highly collimated ions with energies approaching GeV values. Previously, Attwood *et al.* (1978) presented interferometric data that confirmed the significant role of radiation pressure during laser-plasma interaction (10^{23} W/cm^2). Thus, the electrostatic acceleration mechanism

https://doi.org/10.1017/S0263034612000183 Published online by Cambridge University Press

or TNSA and RPA models are mainly applicable for extremely high intensity LTI.

6. CALCULATION OF THE PLASMA PARAMETERS FROM LASER: AG TARGET INTERACTION

The plasma parameters determine how the laser beam interacts with metallic plasma. The plasma parameters depend on the plasma generation and expansion mechanisms. It was shown that the plasma is mostly generated near the target surface. Plasma interaction with a solid surface is complicated. It includes target heating and ablation, generation of high vapor pressure, electron emission from the hot target, and plasma heating and electrical sheath formation at the target-plasma interface (Section 2). Below a self-consistent calculation example that analyzes the physics of laser ablation is presented, taking into account the mentioned above physical phenomena and based on model developed by Beilis (2006, 2007, 2008).

According to the model, the near target plasma flow consists of several physical regions (Fig. 1) including the electrical sheath, a non-equilibrium Knudsen layer, and then a plasma region where the emitted electrons relax. The gas-dynamic Eqs. (4)–(10) were taken in integral form to calculate the velocity V of the accelerated plasma jet. The system of equations (Beilis, 2007) includes the heat-conduction equation for target heating, an equation for the potential drop in the sheath, equations for atom evaporation and electron emission from the target, and target and plasma energy balances. It was taken in account that the laser power density q_L is dissipated not only in the target body but also in the electron relaxation region and in the expanding plasma jet. The plasma parameters were calculated for the conditions in the experiment by Margarone *et al.* (2008) in which a 10 ns, power density $q_L = 10$–100 MW/cm^2 laser beam was incident on a 3 mm^2 spot of an Ag target. The dependencies on q_L was calculated, when for simplicity, the coefficient of power absorption in the plasma jet was taken as a constant $\alpha_{IB} = 0.4$. And, to determine the influence of α_{IB} on the plasma parameters, it was varied while q_L was held constant (Beilis, 2007; Bogaerts *et al.*, 2003). The coefficient of power absorption in the electron relaxation region was taken as $K_e = 0.1$ (Beilis, 2007). The important characteristic is the *evaporation fraction* K_{er} that is the calculated net of target evaporation rate ratio to that rate determined by Langmuir flux into vacuum W_L(Section 3.1).

It was found that the potential drop in the sheath and the electron temperature T_e decrease with increasing q_L (Fig. 2). The target temperature T_0 increases and therefore the target evaporation fraction also increases with q_L (Fig. 3) indicating the vapor non-equilibrium degree at the target. As T_0 increases the heavy particle density n_h also increases, so that the degree of ionization α decreases with increasing q_L (Fig. 4). The emitted electron current density j_e increases by six orders of magnitude while ion current density j_i increases by one order of magnitude with increasing

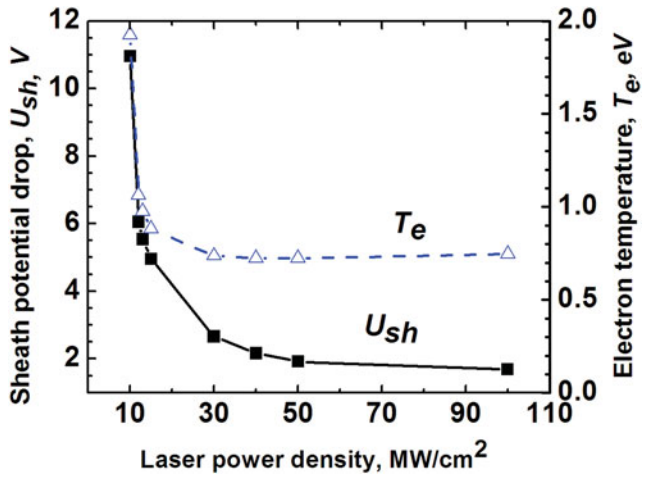

Fig. 2. (Color online) Potential drop in the space charge region near the target surface and plasma electron temperature as a function on laser power density, 10ns pulse.

q_L (Fig. 5). The returned electron current density j_{et} exceeds j_{em} (Fig. 5) so that the total current will be zero for all considered q_L. The electrical field at the target surface increase with q_L to a maximum of 4 MV/cm at $q_L = 15$ MW/cm^2, and then decreased with further increases of q_L, while the target ablation rate G increases by six orders of magnitude with q_L (Fig. 6). G increases because the target temperature increases with q_L. The laser plasma is significantly accelerated by the gas-dynamic mechanism, above 10^6 cm/s and V as well the kinetic jet energy ($mV^2/2$) increase with α_{IB} for constant q_L (Fig. 7). However, when α_{IB}. is constant the velocity V decreases with q_L.

These different dependencies can be understood from relation between α_{IB}, q_L, and n_h in form:

$$V \approx \frac{\alpha_{IB}}{n_h kT} \frac{q_L}{(1 + \alpha T_e/T)}. \tag{15}$$

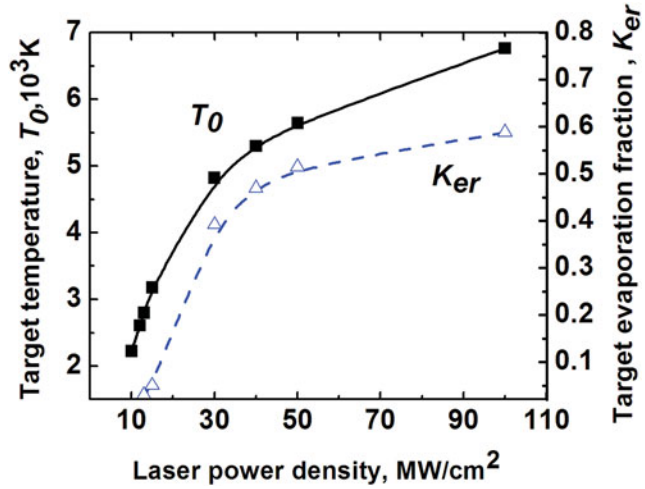

Fig. 3. (Color online) Surface target temperature T_0 and target evaporation fraction K_{er} dependencies on laser power density, 10 ns pulse.

https://doi.org/10.1017/S0263034612000183 Published online by Cambridge University Press

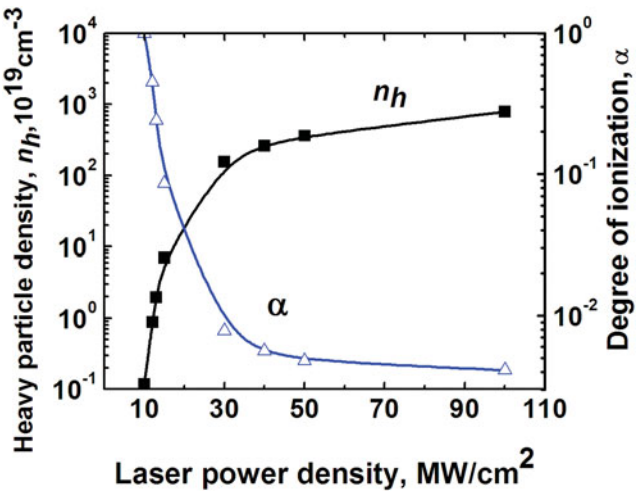

Fig. 4. (Color online) Dependencies of heavy particle density n_h and degree of ionization α in the beam relaxation region as function of laser power density, 10 ns pulse.

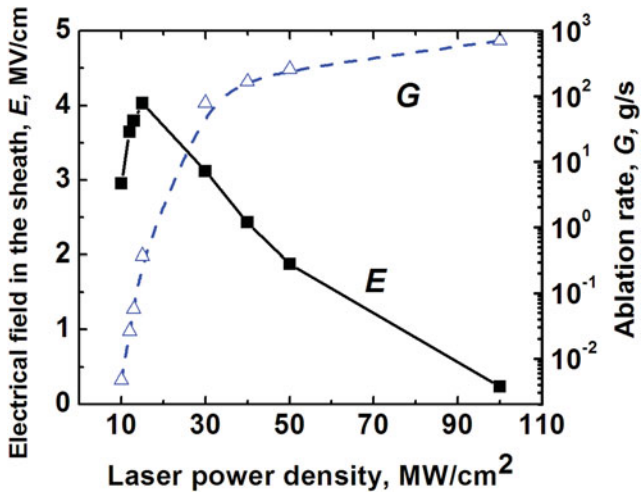

Fig. 6. (Color online) Electric field at the target surface in the sheath and target ablation rate vs. laser power density, 10 ns pulse.

The relation (15) is obtained combining the equations of jet momentum (4) and energy conservation (5) in integral form, taking into account that the absorbed power density $\alpha_{IB}q_L$ causes the plasma heating and its acceleration. The self-consistent calculation shows that the character of heavy particle density dependence on α_{IB} and q_L variation determines the dependence of V. When α_{IB} is constant n_h increase with q_L is significantly larger than the increase of q_L (Fig. 3) and therefore V decreases with q_L, as it follows from Eq. (15), while n_h significantly decreases with α_{IB} for constant q_L and therefore V increases (also see Eq. (15)). The experiments showed that the observed peak energy of different ion species increased with laser energy (Torrisi *et al.*, 2008*a*, 2008*b*, 2002; Caridi *et al.*, 2006). This result indicate that laser energy absorption is non-linearly function on distance in the expanding plasma jet and the plasma velocity is determined by a dependence α_{IB} (x) which, as example, was used by Bogaerts *et al.* (2003) for Cu and power density $>10^8$ W/cm^2.

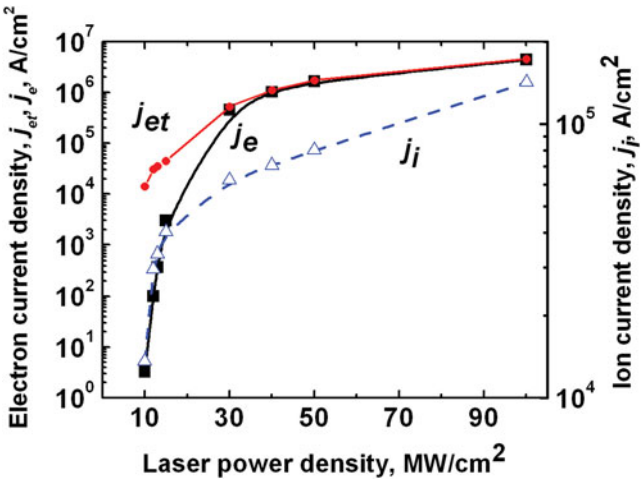

Fig. 5. (Color online) Electron emission j_e, ion j_i and returned electron j_{et} current densities as a function on laser power density, 10 ns pulse.

7. DISCUSSIONS

It may be seen from the LTI experiments and theory described above, that the behavior of the plasma parameters, plasma expansion, and ion acceleration is a result of complex phenomena, which appear during laser plasma formation and development in the kinetic and hydrodynamic regions. The first stage of LTI is characterized by the intense target ablation when mainly neutral atoms were observed and the breakdown of neutral vapor occurs in the second stage producing the laser plasma plume. This transient stage can be understood taking into account the breakdown mechanisms described in Section 3.2. The next stage occurs when the near-target plasma has been produced and the plasma plume expands simultaneously with target heating and ablation, and the part of laser energy dissipated in the plasma. At this stage, the important issue is to determine the plasma parameters, taking into account the mentioned mutual phenomena (Sections 3.1–3.5, 4, and 5) solving the mathematical problem self-consistently. Let us discuss the calculated results at the last stage of LTI.

In general, the present and previous calculations (Beilis, 2007) show that the target vaporizes in a dense near-target plasma that is separated from the solid surface by an electrical sheath with a relatively large potential drop and by a Knudsen layer across, which there is a jump of plasma parameters and a mass flux also toward the target. The electrons emitted from the hot target are accelerated in the sheath. The electron beam energy is dissipated in the electron relaxation region whose length is significantly larger than the length of the Knudsen layer. As result, the plasma flow in the vicinity of the target surface is impeded by the dense plasma and the electron beam energy dissipation. *This is very important in understanding the target ablation rate.* The calculated results for Al and Cu targets (Beilis, 2007, 2008) showed: (1) the dependence of target rate ablation on pulse energy density well agrees with experiments (Caridi *et al.*, 2006); (2) the plasma

https://doi.org/10.1017/S0263034612000183 Published online by Cambridge University Press

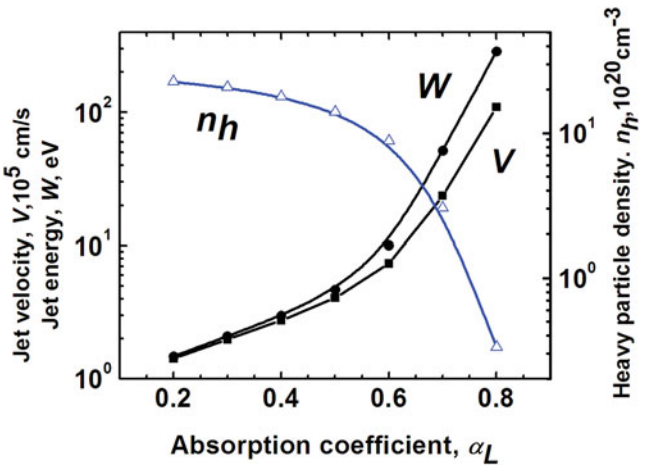

Fig. 7. (Color online) Jet velocity V, jet energy W and heavy particle density n_h as function of coefficient of energy absorption α_L in the plasma jet calculated for *Ag* target with laser pulse 9 ns, $q_L = 33.333 \times MW/cm^2$.

significantly converts the absorbed laser energy to kinetic and potential energy of the plasma particles, which transport part of the energy through the electrostatic sheath back to the solid surface; (3) the energy flux from the adjacent plasma significantly contribute to heating the target; (4) the calculated electron temperature of 1–5 eV agrees well with other calculated results (Bogaerts *et al.*, 2003) and is the range measured by direct spectroscopic methods (see Table 1). This last result is important in understanding the electrostatic fields produced by LTI with moderate power density.

The plasma acceleration depends on the laser energy absorbed in the relaxation region, in the expanding plasma jet and on the rate of target ablation. The calculations show (see also Section 6) that the observed plasma jet velocity can be explained by the gas-dynamic mechanism of plasma acceleration (Beilis, 2007). The distribution of $\alpha_{IB}(x)$ should be taken into account for correctly and quantitatively describe the measured jet velocity increase with laser power density. Inside of the gas-dynamic region (Fig. 1), the dense plasma is quasi-neutral and therefore the electric field is relatively small.

The important issue is to understand the mechanism producing the observed ion energy distribution and the shifted equivalent voltage per charge state. One of the approaches of the previously published works (TNSA, see Section 5) takes into account that the plasma quasi-neutrality is violated and a space charge region with a potential drop U_f (whose value depends on T_e) can appear. Although this mechanism was widely used, the sheath structure was not considered especially, for moderate laser power density when the electron temperature is relatively small, the ion acceleration in the expanding electrical sheath is not detailed. In most cases the characteristic length of the space charge region was chosen to be the Debye length. The electric field E was calculated using the measured shifted equivalent voltage as U_f and Debye length L_D i.e., $E = U_f / L_D$. In this case, the acceleration mechanism remains unknown because namely U_f should be determined. Although the particle acceleration depends on electrical field the particle energy is determined by potential drop in the acceleration region. Note also that Debye length is a parameter characterizes the scale of E where the quasi-neutrality violated and the potential of charged particle interaction about T_e/e. The effect of quasi-neutrality violation takes place also at the expanding plasma front, but the characteristic length depends on the whether the plasma is expanding into vacuum, into a gas or impinges onto a solid wall. In this case, the particle energy acquired by electrostatic acceleration in the space charge region cannot exceed the electron temperature although there is a relatively large electric field in a small region (whose size is the Debye or other length). Therefore the ion acceleration by the electrostatic mechanism described well the experiment with ultra-intense ($>10^{15}$ W/cm^2) laser irradiation when T_e is about MeV. In contrast, for intermediate laser power density, the electrostatic TNSA mechanism cannot explain the observed relatively large ion energy shift per charge because the spectroscopic direct measurements showed that the expanding plasma has relatively low T_e.

The ion acceleration can be described taking into account that there a strong gradient of plasma pressure in the expanding plasma (Zeldovich & Raizer, 1966). The effect of the pressure gradient can be considered by integrating Eq. (13) across some characteristic length in the plasma between distances x_1 and x_2 from the target and taking into account the equation of plasma state. In this case the ion energy increase $\Delta W_{z0} = W_{z0}(x_2) - W_{z0}(x_1)$ with Z_{i0} charge can be obtained in form:

$$\Delta W_{z0} = Z_0\left[\left(\frac{T_i}{Z_0} + T_e\right)Ln\left(\frac{n_{z0}(x_1)}{n_{z0}(x_2)}\right) + \int\sum_{z\neq z0}\frac{n_{iz}}{Z_0 n_{z0}}\left(\frac{dT_i}{dx} + Z\frac{dT_e}{dx}\right)dx + \int\sum_{z\neq z0}\frac{(T_i + ZT_e)}{Z_0 n_{z0}}\frac{dn_{iz}}{dx}dx\right]. \quad (16)$$

And in simple form this dependence is:

$$\frac{\Delta W_{z0}}{Z_0} \sim T_e Ln\left(\frac{n_{z0}(x_1)}{n_{z0}(x_2)}\right) + F(T_e, n_{iz}, Z), \quad (17)$$

where $W_{z0} = mV_{z0}^2/2$ is the ion kinetic energy, Z and Z_0 is the charge of ions with density n_{iz} and n_{iz0}, respectively, $F(T_e,n_{iz},Z)$ is a function expressing the sum of second and third terms on the right side of Eq. (16) and which describes the influence of the pressure gradient for ion charges $Z \neq Z_0$. Eqs. (16) and (17) show that the ion energy linearly depends on the ion charge state, as observed experimentally (Section 2). The ion energy also depends on a jump of plasma parameters produced after the vapor breakdown by laser irradiation. A strong jump of T_e and n_e can appear over a region of few mean free paths at the plasma front (Zeldovich & Raizer, 1966; Raizer, 1974). The simultaneous existence of "hot" electrons and "cold" electrons which

https://doi.org/10.1017/S0263034612000183 Published online by Cambridge University Press

induce rarefaction shock waves with discontinuities in the plasma potential was indicated by Eliezer and Hora (1988). The jump characteristic should be studied taking into account the plasma front interaction with the incident laser pulse.

Another result that should be understood is the relatively wide dispersion observed in the ion energy distribution that increases for ions with larger charge. This dispersion was interpreted as a very large ion temperature, up to about 10^5 K. However, the measurements and calculations show that T_e is low in the dense plasma region, as mentioned above (see Table 1). The plasma is non-equilibrium, i.e., $T_e \neq T$, and the efficiency of energy transfer from the electrons to the heavy particle is too weak to reach equilibrium. One possible interpretation considers that the effect of the wide ion energy distribution is similar to that measured in plasma jets of a vacuum arc (Davis & Miller, 1969). The ion energy distribution in the vacuum arc was explained by superposition of the jets generated by multiple cathode spots (Beilis *et al.*, 1998). It can be taken into account also that the ion energy substantially increases when the erosion rate decreases in arcs with large rate of current or power rise during the discharge pulse (Beilis, 2004).

Thus, similarly to the vacuum arc phenomena, the laser ion energy dispersion can be explained taking into account the different plasma jet parameters generated, for example, in experiments with multi-pulse laser irradiation of the target. In this case the plasma parameters produced by a laser pulse depends on the target surface features produced by the previous pulse. Indeed, roughening of Si surfaces treated by nanosecond laser pulses was shown by Schwarz-Selinger *et al.* (2001). Consequently, the plasma parameters are determined by the vaporization rate of surface irregularities and a target erosion rate will not be uniform. Surface non-uniformity causes the observed ion energy variation because the ion acceleration depends on the target local erosion rate, which depends on the local target surface morphology. The morphology varies during a single pulse and from pulse to pulse. The origin of ion energy variation can be explained taking into account the large incoming laser power intensity in short laser pulses and the mechanism of ion acceleration depending on target ablation rate by analogy to the cathode erosion rate in arcs (Beilis, 2004). It should be noted that plasma structure formation due to non-uniformity of power density distribution within the laser spot in single laser pulse also was indicated by Hora (1981).

ACKNOWLEDGMENT

The author would like to thank to Prof. R.L. Boxman for useful discussion improving the paper presentation.

REFERENCES

Abdellatif, G. & Imam, H. (2002). A study of the laser plasma parameters at different laser wavelengths. *Spectrochimica Acta* **B57**, 1155.

Aden, M., Beyer, E. & Herziger, G. (1990). Laser-induced vaporization of metal as a Riemann problem. *J. Phys. D: Appl. Phys.* **23**, 655.

Aguilera, J.A., Bengoechea, J. & Arago., C. (2004). Spatial characterization of laser induced plasmas obtained in air and argon with different laser focusing distances. *Spectrochimica Acta* **B59** 461.

Anisimov, S.I., Bauerly, D. & Luk'yanchuk, B.S. (1993). Gas dynamics and film profiles in pulsed laser deposition of materials. *Phys. Rev.* **B48**, 12076–12081.

Anisimov, S.I., Imas, Yu.A., Romanov, G.S. & Khodyko, Yu.V. (1971). *Action of High-Power Radiation on Metals*. Springfield, VA: National Technological Information Service.

Anisimov, S.I. (1968). Vaporization of metal absorbing laser radiation. *Sov. Phys. JETP* **37**, 182–183.

Attwood, D.T., Sweeney, D.W., Auerbach, J.M. & Lee, P.H.Y. (1978). Interferometric confirmation of radiation-pressure effects in laser-plasma interactions. *Phys. Rev. Lett.* **40**, 184.

Beilis, I.I. (1974). Emission processes at the cathode of an electric arc. *Sov. Phys. Tech. Phys.* **19**, 257.

Beilis, I.I. (1982). On the theory of the erosion processes in the cathode region of an arc discharge. *Sov. Phys. Doklady* **27**, 150–152.

Beilis, I.I. (1985). Parameters of kinetic layer of arc discharge cathode region. *IEEE Trans. Plasma Sci.* **PS-13**, 288.

Beilis, I.I. (1986). Cathode arc plasma flow in a Knudsen layer. *High Temp.* **24**, 319.

Beilis, I.I. (1995). "Theoretical modelling of cathode spot phenomena." In *Handbook of Vacuum Arc Science and Technology* (ed. R.L. Boxman P.J. Martin D.M. Sanders). Park Ridge, N.J: Noyes Publishing, 208–256.

Beilis, I.I. (2001). State of the theory of vacuum arcs. *IEEE Trans. Plasma Sci.* **29**, 657–670.

Beilis, I.I. (2003). The vacuum arc cathode spot and plasma jet: Physical model and mathematical description. *Plasma Phys.* **43**, 224–236.

Beilis, I.I. (2004). Nature of high-energy ions in the cathode plasma jet of a vacuum arc with high rate of current rise. *Appl. Phys. Lett.* **85**, 2739.

Beilis, I.I. (2006). Mechanism of laser plasma production and of plasma interaction with a target. *Appl. Phys. Lett.* **89**, 091503.

Beilis, I.I. (2007). Laser plasma generation and plasma interaction with ablative target. *Laser Part. Beams* **25**, 53–63.

Beilis, I.I. (2008). Metallic plasma production by laser ablation. *Radi. Effects Defects Solids* **163**, 317.

Beilis, I.I., Keidar, M., Boxman, R.L. & Goldsmith, S. (1998). Theoretical study of plasma expansion in a magnetic field in a disk anode vacuum arc. *J. Appl. Phys.* **83**, 709.

Beilis, I.I. & Keidar, M. (1998). Sheath and presheath structure in the plasma wall-transition layer in an oblique magnetic field. *Phys. Plasmas* **5**, 1545.

Bhatnagar, P.L., Cross, E.P. & Krook, M. (1954). A model for collision processes in gases. I. Small amplitude processes in charged and neutral one-component systems. *Phys. Rev.* **94**, 511.

Bleiner, D., Bogaerts, A., Beiloni, F. & Nassisi, V. (2007). Laser-induced plasmas from the ablation of metallic targets: The problem of the onset temperature, and insights on the expansion dynamics. *J. Appl. Phys.* **101**, 083301.

Bogaerts, A., Chen, Z., Gijbels, R. & Vertes, A. (2003). Laser ablation for analytical sampling: What can we learn from modeling? *Spectrochimica Acta.* **B58**, 1867–1893.

Bohm, D. (1949). *Characteristics of Electrical Discharges in Magnetic Fields*. New York: Mcgraw-Hill Book Company, Inc.

Caretto, G., Doria, D., Nassisi, V. & Siciliano, M.V. (2007). Photoemission studies from metal by UV lasers. *J. Appl. Phys.* **101**, 073109.

Caridi, F., Torrisi, L., Margarone, D., Picciotto, M., Mezzasalma, A.A. & Gammino, S. (2006). Energy distributions of particles ejected from laser generated pulsed plasmas. *Czech. J. Phys.* **56** B449–B455.

Chang, J.J. & Warner, B.E. (1996). Laser-plasma interaction during visible-laser ablation of methods. *Appl. Phys. Lett.* **69**, 22.

Chen, Z. & Bogaerts, A. (2005). Laser ablation of Cu and plume expansion into 1 atm ambient gas. *J. Appl. Phys.* **97**, 063305.

Chen, M., Liu, X., Yanga, X., Zhao, M., Sun, Y, Qi, H., Chenc, X. & Xu, X. (2008). The dimension of the core and the tail of the plasma produced by laser ablating SiC targets. *Phys. Lett.* **A372**, 5891.

Chen, M., Liu, X., Zhao, M., Chen, C. & Man, B. (2009*a*). Temporal and spatial evolution of Si atoms in plasmas produced by a nanosecond laser ablating silicon carbide crystals. *Phys. Rev.* **E80**, 016405.

Chen, M., Liu, X., Zhao, M. & Sun, Y. (2009*b*). Early-stage evolution of the plasma over KTiOPO4 samples generated by high-intensity laser radiations. *Opt. Lett.* **34**, 2682.

Corsi, M., Cristoforetti, G., Giuffrida, M., Hidalgo, M., Legnaioli, S., Palleschi, V., Salvetti, A., Tognoni, E. & Vallebona, C. (2004). Three-dimensional analysis of laser induced plasmas in single and double pulse configuration. *Spectrochimica Acta Part* **B59**, 723.

Cristoforetti, G., Lorenzetti, G., Benedetti, P.A., Tognoni, E., Legnaioli, S. & Palleschi, V. (2009). Effect of laser parameters on plasma shielding in single and double pulse configurations during the ablation of an aluminium target. *J. Phys. D: Appl. Phys.* **42**, 225207.

Davis, W.D. & Miller, C.H. (1969). Analysis of the electrode products emitted by dc arcs in a vacuum ambient. *J. Appl. Phys.* **40**, 2212.

Denavit, J. (1979). Collisionless plasma expansion into vacuum. *Phys. Fluids* **B22**, 1384.

Devies, J.R., Bell, A.R. & Tatarakis, M. (1999). Magnetic focusing and trapping of high-intensity laser-generated fast electrons at the rear of solid targets. *Phys. Rev.* **E59**, 6032.

Dubey, A.K. & Yadava, V. (2008). Laser beam machining—A review. *Intern. J. Mach. Tools & Manufact.* **48**, 609.

Dolan, W.W. & Dyke, W.P. (1954). Temperature and field emission of electrons from metals. *Phys. Rev.* **95**, 327.

Eliezer, S., Eliaz, N., Grossman, E., Fisher, D., Gouzman, I., Henis, Z., Pecker, S., Horovitz, Y., Fraenkel, M., Maman, S., Ezersky, V. & Eliezer, D. (2005). Nanoparticles and nanotubes induced by femtosecond lasers, *Laser Part. Beams* **23**, 15–19.

Eliezer, S. & Ludmirsky, A. (1983). Double layer formation in laser produced plasma. *Laser Part. Beams* **1**, 251–269.

Eliezer, S. & Hora, H. (1988). Double layers in laser produced plasma. *Phys. Repts.* **172**, 339–406.

Fernandez, J.C., Hegelich, B.M., Cobble, J.A., Flippo, K.A., Letzring, S.A., Johnson, R.P., Gautier, D.C., Shimada, T., Kyrala, G.A., Wang, Y., Wetteland, C.J. & Schreiber, J. (2005). Laser-ablation treatment of short-pulse laser targets: Toward an experimental program on energetic-ion interactions with dense plasmas. *Laser Part. Beams* **23**, 267–273.

Fisher, J. (1976). Distribution of pure vapor between two parallel plates under the influence of strong evaporation and condensation. *Phys. Fluids* **19**, 1305.

Franghiadakis, Y., Fotakis, C. & Tzanetakis, P. (1999). Energy distribution of ions produced by excimer-laser ablation of solid and molten targets. *Appl. Phys.* **A68**, 391–397.

Franklin, R.N. (2003). The plasma–sheath boundary region. *J. Phys. D: Appl. Phys.* **36**, R309.

Gamaly, E.G. (1993). The interaction of ultrashort, powerful laser pulses solid target: Ion expansion and acceleration with time-dependent ambipolar field. *Phys. Fluids* **B5**, 944.

Gamaly, E.G., Luther-Davies, B., Kolev, V.Z., Madsen, N.R., Duering, M. & Rode, A.V. (2005). Ablation of metals with picosecond laser pulses: Evidence of long-lived non-equilibrium surface states. *Laser Part. Beams* **23**, 167–176.

Gamaly, E.G. Rodea, A.V. & Luther-Davies, B. (1999). Ultrafast ablation with high-pulse-rate lasers. Part I: Theoretical considerations. *J. Appl. Phys.* **85**, 4213–4221.

Gamaly, E.G., Rode, A.V., Luther-Davies, B. & Tikhonchuk, V.T. (2002). Ablation of solids by femtosecond lasers: Ablation mechanism and ablation thresholds for metals and dielectrics. *Phys. Plasmas* **9**, 949.

Gili, D.H. & Dougal, A.A. (1965). Breakdown minima due to electron-impact ionization in super-high-pressure gases irradiated by a focused giant-pulse laser. *Phys. Rev. Lett.* **15**, 845.

Gusarov, A.V., Gnedovets, A.G. & Smurov, I. (2000). Gas dynamics of laser ablation: Influence of ambient atmosphere. *J. Appl. Phys.* **88**, 4352.

Gusarov, V. & Aoki, K. (2005). Ionization degree for strong evaporation of metals. *Phys. Plasmas* **12**, 083503.

Hafez, M.A., Khedr, M.A., Elaksher, F.F. & Gamal, Y.E. (2003). Characteristics of Cu plasma produced by a laser interaction with a solid target. *Plasma Sour. Sci. Technol.* **12**, 185.

Hatchett, S.P., Brown, C.G., Cowan, T.E., et al. (2000). Electron, photon, and ion beams from the relativistic interaction of petawatt laser pulses with solid targets. *Phys. Plasmas* **7**, 2076.

Hegelich, M., Karsch, S., Pretzler, G., Habs, D., Witte, K., Guenther, W., Allen, M., Blazevic, A., Fuchs, J., Gauthier, J.C., Geissel, M., Audebert, P., Cowan, T. & Roth, M. (2002). MeV ion jets from short-pulse-laser interaction with thin foils. *Phys. Rev. Lett.* **89**, 085002.

Henc-Bartolic, V., Andreic, Z. & Kunze, H.J. (1994). Titanium plasma produced by a nitrogen laser. *Phys. Scripta* **50**, 368.

Henc-Bartolic, V., Boncina, T., Jakovljevic, S., Pipic, D. & Zupanic, F. (2008). The action of a laser on an aluminium target. *Mater. Technol.* **42**, 111.

Hermann, J., Thomann, A.L., Leborgne, C. & Dubreuil, B. (1995). Pulsed diagnostics in pulsed laser TiN layer deposition. *J. Appl. Phys.* **77**, 2928–2936.

Hoffmann, D.H.H., Blazevic, A.P., Rosmej, N.O. Roth, M. Tahir, N.A., Tauschwitz, A., Udrea, S., Varentsov, D., Weyrich, K. & Maron, Y. (2005). Present and future prospective for high energy density physics with intense heavy ion and laser beams. *Laser Part. Beams* **23**, 47–53.

Hora, H. (1981). *Physics of Laser Driven Plasmas*. New York: John Wiley.

Itina, T.E., Hermann, J., Delaporte, Ph. & Sentis, M. (2002). Laser-generated plasma plume expansion: Combined continuous-microscopic modeling. *Phys. Rev.* **E66**, 066406.

Kasperczuk, A., Pisarczyk, T., Kalal, M., Martinkova, M., Ullschmied, J., Krousky, E., Masek, K., Pfeifer, M., Rohlena,

K., Skala, J. & Pisarczyk, P. (2008). PALS laser energy transfer into solid targets and its dependence on the lens focal point position with respect to the target surface. *Laser Part. Beams* **26**, 189–196.

Keidar, M., Beilis, I.I., Boxman, R.L. & Goldsmith, S. (1996). 2-D expansion of the low density interelectrode vacuum arc plasma in an axial magnetic field. *J. Phys. D: Appl. Phys.* **29**, 1973.

Keidar, M., Boyd, I.D. & Beilis, I.I. (2001). On the model of Teflon ablation in an ablation-controlled discharge. *J. Phys. D: Appl. Phys.* **34**, 1675.

Keidar, M. & Beilis, I.I. (2005). Transition from plasma to space-charge sheath near the electrode in electrical discharges. *IEEE Trans. Plasma Sci.* **33**, 1481.

Knudsen, M. (1915). Die Maximale Verdampfungsgeschwindigkeit des Quecksilbers (The rate of mercury evaporation). *Ann. Phys. Chem.* **47**, 697.

Langmuir, I. & Mackay, J.M.G. (1914). The vapor pressure of the metals platinum and molybdenum. *Phys. Rev.* **4** 377.

Langmuir, I. (1929). The interaction of electron and positive ion space charges in cathode sheaths. *Phys. Rev.* **33** 954.

Liseikina, T.V., Prellino, D., Cornolti, F. & Macchi, A. (2008). Ponderomotive acceleration of ions: Circular versus linear polarization. *IEEE Trans. Plas. Sci.* **36**, 1866.

Margarone, D., Torrisi, L., Borrielli, A. & Caridi, F. (2008). Silver plasma by pulsed laser ablation. *Plasma Sour. Sci. Techol.* **17**, 035019.

Mazhukin, V.I., Nossov, V.V., Nickiforov, M.G. & Smurov, I. (2003). Optical breakdown in aluminum vapor induced by ultraviolet laser radiation. *J. Appl. Phys.* **93**, 56.

Miller, G.H., Moses, E.I. & Wuest, C.R. (2004). The National Ignition Facility: enabling fusion ignition for the 21st century. *Nucl. Fusion* **44**, 228.

Moscicki, T., Hoffman, J. & Szymanski, Z. (2006). Modelling of plasma plume induced during laser welding. *J. Phys. D: Appl. Phys.* **39**, 685–692.

Pearlman, J.S., Morse, B.L. (1978). Maximum expansion velocities laser plasmas. *Phys. Rev. Lett.* **40**, 1652.

Popov, S., Panchenko, A., Batrakov, A., Ljubchenko, F. & Mataibaev, V. (2011). Experimental Study of the Laser Ablation Plasma Flow from the Liquid Ga-In Target. *IEEE Trans. Plasma Sci.* **39**, 1412.

Pukhov, A. (2001). Three-dimensional simulations of ion acceleration from a foil irradiated by a short-pulse laser. *Phys. Rev. Lett.* **86**, 3562.

Raizer Yu, P. (1974). *Laser Spark and Discharge Expansion*. Moscow: Nauka.

Raizer Yu, P. (1965). Breakdown and heating of gases under the influence of a laser beam. *Sov. Pys. Uspekhy* **8**, 650.

Raizer Yu, P. (1980). Optical discharges. *Sov. Phys. Uspekhy* **23**, 789.

Rieger, G.W., Taschuk, M., Tsui, Y.Y. & Fedosejevs, R. (2003). Comparative study of laser-induced plasma emission from microjoule picosecond and nanosecond KrF-laser pulses. *Spectrochim. Acta* **B58**, 497.

Rosen, D.I., Mitteldorf, J., Kothandaraman, G., Pirri, A.N. & Pugh, E.R. (1982). Coupling of pulsed 0.35-μm laser radiation to aluminum alloys. *J. Appl. Phys.* **53**, 3190.

Singh, R.K. & Narayan, J. (1990). Pulsed-laser evaporation technique for deposition of thin films: Physics and theoretical model. *Phys. Rev.* **B41**, 8843–8859.

Schaumann, G., Schollmeier, M.S., Rodriguez-Prieto, G., Blazevic, A., Brambrink, E., Geissel, M., Korostiy, S., Pirzadeh, P., Roth, M., Rosmej, F.B., Faenov, A.Y., Pikuz, T.A., Tsigutkin, K., Maron, Y., Tahir, N.A. & Hoffmann, D.H.H. (2005). High energy heavy ion jets emerging from laser plasma generated by long pulse laser beams from the NHELIX laser system at GSI. *Laser Part. Beams* **23**, 503.

Schwarz-Selinger, T., Cahill, D.G., Chen, S.-C., Moon, S.-J. & Grigoropoulos, C.P. (2001). Micron-scale modifications of Si surface morphology by pulsed-laser texturing. *Phys. Rev.* **B64**, 155323.

Shoucri, M., Lavocat-Dubuis, Matte, X.J-P. & Vidal, F. (2011). Numerical study of ion acceleration and plasma jet formation in the interaction of an intense laser beam normally incident on an overdense plasma. *Laser Part. Beams* **29**, 315–332.

Shukla, G. & Khare, A. (2010). Spectroscopic studies of laser ablated ZnO plasma and correlation with pulsed laser deposited ZnO thin film properties. *Laser Part. Beams* **28**, 149–155.

Steinke, S., Henig, A., Schnurer, M., Sokollik, T., Nickles, P.V., Jung, D., Kiefer, D., Horlein, R., Schreiber, J., Tajima, T., Yan, X.Q., Hegelich, M., Meyer-ter-Vehn, J., Sandner, W. & Habs, D. (2010). Efficient ion acceleration by collective laser-driven electron dynamics with ultra-thin foil targets. *Laser Part. Beams* **28**, 215–221.

Sun, Y., Chen, M., Li, Y., Qi, H., Zhao, M. & Liu, X. (2008). Analysis of plasma profile over KTiOAsO4 surface produced by 532 and 1064 nm laser radiations. *J. Appl. Phys.* **104**, 123303.

Torrisi, L., Ciavola, G., Gammino, S., Ando, L. & Barna, A. (2000). Metallic etching by high power Nd:yttrium–aluminum–garnet pulsed laser irradiation. *Rev. Scientific Instrum.* **71**, 4330.

Torrisi, L., Ando, L., Ciavola, G., Gammino, S. & Barna, A. (2001). Angular distribution of ejected atoms from Nd:YAG laser irradiating metals. *Rev. Sci. Instrum.* **72**, 68.

Torrisi, L., Gammino, S., Ando, L. & Laska, L. (2002). Tantalum ions produced by 1064 nm pulsed laser irradiation. *J. Appl. Phys.* **91**, 4685.

Torrisi, L. & Gammino, S. (2006). Method for the calculation of electrical field in laser-generated plasma for ion stream production. *Rev. Sci. Instrum.* **77**, 03B707.

Torrisi, L., Caridi, F., Margarone, D., Picciotto, A., Mangione, A. & Beltrano, J.J. (2006). Carbon-plasma produced in vacuum by 532 nm–3 ns laser pulses ablation. *Appl. Surf. Sci.* **252**, 6383.

Torrisi, L., Caridi, F., Margarone, D. & Borrielli, A. (2008*a*). Plasma-laser characterization by electrostatic mass quadrupole analyzer. *Nucl. Instrum. Meth. Phys. Res.* **B266**, 308.

Torrisi, L., Caridi, F., Margarone, D. & Borrielli, A. (2008*b*). Characterization of laser-generated silicon plasma. *Appl. Surf. Sci.* **254**, 2090.

Tajima, T. & Dawson, J.M. (1979). Laser electron accelerator. *Phys. Rev. Lett.* **43**, 267.

Tsue, Y.Y. & Redman, D.G. (2000). A laser ablation technique for improving the adhesion of laser-deposited diamond-like carbon coatings to metal substrates. *Surf. Coat. Technol.* **126** N2–3 96.

Wang, Hai-Xing, & Chen, Xi. (2003). Three-dimensional modelling of the laser-induced plasma plume characteristics in laser welding. *J. Phys. D: Appl. Phys.* **36**, 628.

Wickens, L.M., Allen, J.E. & Rumsby, P.T. (1978). Ion emission from laser-produced plasmas with two electron temperatures. *Phys. Rev. Lett.* **41**, 243.

Wilks, S.C., Langdon, A.B., Cowan, T.E., Roth, M., Singh, M., Hatchett, S., Key, M.H., Pennington, D., MacKinnon, A. & Snavely, R.A. (2001). Energetic proton generation in ultra-intense laser–solid interactions. *Phys. Plasmas* **8**, 542.

Zeldovich, Ya.B. & Raizer, Yu.P. (1966). *Physics of shock waves and high-temperature hydrodynamic phenomena*. New York: Academic Press.

Zheng, J.P., Huang, Z.Q., Shaw, D.T. & Kowk, H.C. (1989). Generation high-energy atomic beams laser. *Appl. Phys. Lett.* **54**, 280–282.

Zeng, X., Mao, X., Mao, S.S., Wen, Sy-Bor, Greif, R. & Russo, R.E. (2006). Laser-induced shockwave propagation from ablation in a cavity. *Appl. Phys. Lett.* **88**, 061502.

https://doi.org/10.1017/S0263034612000183 Published online by Cambridge University Press